Crystal Shape Modification via Cycles of Growth and Dissolution in a Tubular Crystallizer

Peter Neugebauer,[†] Javier Cardona,[‡] Maximilian O. Besenhard,[§,‖] Anna Peter,[‖] Heidrun Gruber-Woelfler,[†,‖] Christos Tachtatzis,[‡] Alison Cleary,[‡] Ivan Andonovic,[‡] Jan Sefcik,[⊥] and Johannes G. Khinast*,[†,‖]

[†]Graz University of Technology, Institute of Process and Particle Engineering, Inffeldgasse 13, 8010 Graz, Austria

[‡]Centre for Intelligent Dynamic Communications, Department of Electronic and Electrical Engineering, University of Strathclyde, Royal College Building, 204 George Street, Glasgow, G1 1XW, U.K.

[§]Department of Chemical Engineering, University College London, Torrington Place, London, WC1E 7JE, U.K.

[‖]Research Center for Pharmaceutical Engineering (RCPE) GmbH, Inffeldgasse 13, 8010 Graz, Austria

[⊥]Department of Chemical and Process Engineering, University of Strathclyde, 75 Montrose Street, Glasgow, G1 1XJ, U.K.

S *Supporting Information*

ABSTRACT: Besides size and polymorphic form, crystal shape takes a central role in engineering advanced solid materials for the pharmaceutical and chemical industries. This work demonstrates how multiple cycles of growth and dissolution can manipulate the habit of an acetylsalicylic acid crystal population. Considerable changes of the crystal habit could be achieved within minutes due to rapid cycling, i.e., up to 25 cycles within <10 min. The required fast heating and cooling rates were facilitated using a tubular reactor design allowing for superior temperature control. The face-specific interactions between solvent and the crystals' surface result in face-specific growth and dissolution rates and hence alterations of the final shape of the crystals in solution. Accurate quantification of the crystal shapes was essential for this work, but is everything except simple. A commercial size and shape analyzer had to be adapted to achieve the required accuracy. Online size, and most important shape, analysis was achieved using an automated microscope equipped with a flow-through cell, in combination with a dedicated image analysis routine for particle tracking and shape analysis. Due to the implementation of this analyzer, capable of obtaining statistics on the crystals' shape while still in solution (no sampling and manipulation required), the dynamic behavior of the size shape distribution could be studied. This enabled a detailed analysis of the solvent's effect on the change in crystal habit.
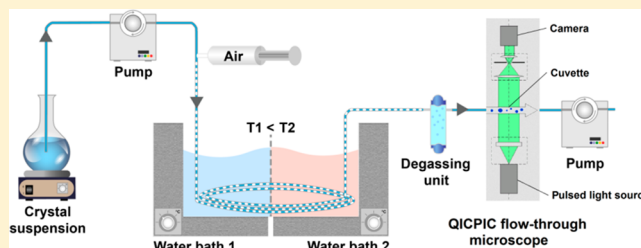
1. INTRODUCTION

In addition to being a technique for separation and purification, crystallization from solution has become an important tool for the production of advanced solid materials with well-defined, "engineered" properties. Depending on the respective end-use of crystalline materials, crystal engineering targets three key aspects that determine the functionality/quality of the material: (i) crystal size and size distribution, including the issue of fines material minimization, (ii) control of molecular arrangement in the crystal lattice (polymorphic state) and the associated defect structure, and (iii) the crystal shape distribution. The first two issues have received much attention for many decades. Recently, however, shape control (i.e., control of the crystal habit) has become a field of increasing interest due to its central importance for specialty applications. Handling and mechanical stability issues, as well as difficulties associated with solid−liquid separation, are concerns for certain shapes, including needles, acicular or dendritic shapes, platelets, or flakes. Thus, a robust three-

dimensional growth to form stout crystals of approximately similar dimensions is the desired mode of crystal formation. For some applications, however, high specific surface areas are desired, e.g., associated with platelike or reticulated crystal shapes, since this enhances the dissolution rates of dissolution-rate limited APIs. Also other specific applications make use of fragile crystal forms, e.g., ZnO nanowires in solar cells.[1] Besides geometric preferences, the changing presence and relative exposure of different crystal faces influences face-specific properties. Molecular crystals expose different sets of atoms or functional groups on each face, causing different interactions with the environment, e.g., the solute and solvent molecules. For example, the wetting behavior of crystal faces, being related to the specific surface energy via Young's equation, has shown to be anisotropic.[2] Other properties of interest for the

pharmaceutical industry are the dissolution behavior,[3] the catalytic potential, and the chemical stability.[4]

During crystallization, many parameters govern the final shape of the product. Early studies correlated the final shape with the internal structure of the crystalline lattice.[5,6] In the case of strong lateral interactions between molecules of a certain face, the surface density increases, leading to higher stabilities and slower perpendicular growth rates of the respective face. Therefore, it eventually becomes a dominant face.[7] Early research about the interaction of molecules in the solid state facilitated equilibrium shape calculations using force-fields implemented in computer programs, such as HABIT[8] and Morang.[9] Yet, these theoretical approaches could not take into account the influence of foreign molecules, such as the solvent, and, therefore, could not predict the shape of solution-grown crystals. Factors, such as solvent, additives, impurities, and supersaturation, impact the mechanism of the incorporation of molecules into the crystal's surface, which is neglected by these models. The mechanism of crystal growth can change between spiral growth, 2D nucleation and growth, and rough growth—all differing in terms of rate of incorporation of solute molecules into the crystalline lattice.[10,11] Microscopic techniques can be used to determine each face's steady-state growth kinetics, based on the measured crystal size and shape distributions under constant process conditions.[12,13] A priori predictions of the exact perpendicular growth rates for each face of a faceted crystal (e.g., using the Frank-Chernov condition[14,15]), though, are still not feasible, particularly regarding the influence of supersaturation. At low supersaturations the formation of stable 2D nuclei is limited due to the high thermodynamic free-energy barrier and spiral growth is the prevailing mechanism.[13,16,17] Kink sites, being positions where molecules will incorporate most readily on the surface, appear only in a small number on flat faces during spiral growth. Therefore, respective growth rates are low. At high supersaturations, growth rates are at least 1 order of magnitude higher. This is due to a high surface nucleation rate and the high density of kink sites present, resulting in so-called "rough growth".[12] The transition between these mechanisms, though, is hard to predict.

Also, the number of kink sites on a specific surface of a crystal is not only influenced by the supersaturation: All molecules present in a given solution will interact with a crystal's surface. In the case of molecules for which the free energy of the system decreases upon interaction, the number of kink sites on the respective face is increased (and vice versa in the case of dissimilar molecules).[7] An overview of solvent effects can be found in the work of Lahav and Leiserowitz[10] and Davey[18] and is reviewed in the paper of Lovette et al.[12] There, the role of the mechanism with the fastest perpendicular growth rate for each face is emphasized as it decides whether the respective face appears in the steady-state shape (if the growth rate is small relative to the other faces) or not (if the growth rate is high).

Due to the many parameters influencing the incorporation of molecules into a surface in a yet unclear manner, modeling depends on certain simplifications. For example, Zhang et al.,[19] while modeling the shapes of a population of crystals grown in a homogeneous solution, assumed constant kink free energies over the whole crystallization process. The associated calculations resulted in crystals developing toward a fixed (steady-state) shape.[7,13,19,20]

In the present work, the attainable shapes of acetylsalicylic acid crystals are investigated when exposed to cycles of growth and dissolution using a tubular crystallizer. In contrast to experiments where growth alone determines the final shape of a crystal population, the number of attainable shapes is significantly expanded, due to crystal dissolution mechanisms differing from mechanisms of crystal growth.[21] In contrast to crystal growth, during dissolution, crystal shapes are generally dominated by fast moving planes or, in other words, the planes with the fastest rate of dissolution will eventually become visible/dominant. This was elaborated by Snyder and Doherty,[11] discussing mechanisms of dissolution at low undersaturation in detail. Similar to crystal growth, concerning most real organic crystals, at low undersaturation, the spiral dislocation mechanism is prevailing, whereas, at higher undersaturation, 2-D nuclei become the main source of steps and kinks.

Unique for dissolution, though, is the event of creating new faces bifurcating from edges and vertices. These stepped and kinked faces are assumed to have not only high relative perpendicular growth rates but also high relative dissolution rates (due to the great increase in the density of kink sites).[7] Therefore, during growth they become "virtual" faces and are not visible in the habit of the crystal, but eventually become dominant during dissolution.

On the basis of the 3D evolution models developed by Snyder et al.,[22] numerous different shapes can appear for a faceted crystal after multiple cycles of growth and dissolution (assuming regrowth to the original crystal volume after each cycle). Clearly, the central requirement for a shape change to happen is that the rates of growth and dissolution for at least one crystal face are not equal. This can be realized via one of the following ways: (I) As discussed above, additives and specific solvents have face-specific interactions with the crystal surface. This interaction will generally be less important for dissolution, resulting in unequal rates. (II) Different mechanisms for growth and dissolution may occur due to super/undersaturation effects. (III) During dissolution, faces which are present at the steady-state growth shape might disappear, therefore becoming "virtual" faces. During regrowth, these faces show different perpendicular growth rates until they reappear on the surface. Simultaneously, new faces might appear during dissolution due to bifurcating edges and vortices.

In the present work, cycles of growth and dissolution for a starting population of acetylsalicylic acid (ASA) crystals suspended in their saturated solution resulted in a change of shape via usage of solvents of different polarities. The known crystal morphologies of ASA grown in different solvents can be found in the literature. Following the indexing by Aubrey-Medendorp et al.,[23] throughout this work, the major face appearing during ASA crystal growth is referred to as the (100) and the (001) face, besides three minor faces, referred to as the (001) face, the (011) face, and the (110) face;[24] see Figure 1.

The relative exposure of these faces, though, is strongly influenced by the solvent in which crystals grow. Polar solvents, such as ethanol, methanol, and acetone, were shown to result in platelike crystals of ASA with the (100) face having the largest surface area. Nonpolar solvents like hexane and n-heptane are reported to yield needle- or rodlike shapes, with fast molecule addition remaining on the (011) face, therefore becoming a small face relative to the major face.[24−27] The interaction of solvent molecules with the ASA crystal's faces was investigated for ethanol and hexane using molecular
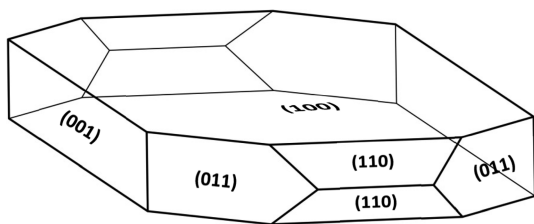
Figure 1. Growth morphology of acetylsalicylic acid (Adapted from ref 23. Copyright 2018, Elsevier).

dynamics simulations.[28] According to the specific arrangement of strong H-bonds between ASA molecules' carboxyl groups in the crystal, their exposure on the (100) face is unfavorable, leading to the (100) face being less hydrophilic, i.e., less polar, than the (001) face. Therefore, while being in contact with a polar solvent like ethanol, growth on the (100) face occurs in a layer-by-layer manner, being the most unfavorable growth mechanism. The more hydrophilic nature of the (001) face prefers the interaction with a polar solvent, and thus, growth along this face is accelerated when in contact with ethanol. Growth rates on this plane are expected to decelerate with decreasing polarity of the solvent due to a loss of crystal order on the surface. Hence, crystal growth depends on bigger building blocks, being limited by slower diffusion rates to the crystals surface. The presence of both hydrophilic hydroxyl groups and hydrophobic phenyl groups on the (011) plane generates a more stable surface structure in both polar (ethanol) and nonpolar (hexane) solvents. This enables fast single molecular addition.[23,28]

In this study, the first set of experiments focused on a single solvent (ethanol) to induce shape tuning by applying 5, 10, 15, 20, and 25 temperature cycles We show that a continuously operated crystallizer, including a setup for temperature cycling, can alter the habit of a crystalline population due to the relative rates of growth and dissolution of various crystal faces. In a second set of experiments, we focused on the effect of three different solvents to induce shape tuning by applying 25 temperature cycles within a short time range of several minutes. The individual effect of ethanol, isopropanol, and hexanol, which are part of the homologous series of alcohols, was compared. The experimental studies of the dynamic change of crystal shapes were facilitated by the implementation of an automated microscope and the development of a dedicated particle tracking and shape analysis routine.

2. MATERIALS AND METHODS

2.1. Setup and Equipment. In the present study, cycles of growth and dissolution are made possible using a continuous tubular crystallizer setup. Among many advantages of tubular crystallizers, substantiated experimentally in earlier publications of our group,[29−39] high heat-transfer rates enable fast temperature changes and, therefore, changes of the saturation. A setup allowing rapid change of the saturation levels, with the aim to continuously engineer crystals, has been presented recently[40] and was adapted for this study, focusing on shape tuning and online image analysis. A schematic of the tubular temperature cycler is given in Figure 2. To implement alternating heating and cooling stages for dissolution and growth of crystals, water baths were used in which successive parts of the tubular crystallizer were immersed.

In the setup, a polysiloxane tubing with an inner diameter of $d_{in} = 2$ mm was used, cycling the crystal suspension between water baths, resulting in sections of 1.86 m per cycle (2×83 cm inside the cold and warm water baths, and 2×10 cm for the connections in between). For each loop, the suspension first passed the section immersed in the cold bath, followed by the warm water bath. Depending on the respective experiment, the overall number of loops varied from 5 to 25, with 1 m of tube at the inlet and 1 m at the outlet. The maximum overall length therefore was 48.5 m.

To achieve controlled transport of crystals in the crystallizer, a segmented flow was established. Using two syringe pumps (LA-120, HLL Landgraf, Germany), a continuous air supply to the crystallizer was facilitated via a T-fitting. The suspension was pumped through the tubing using a peristaltic pump (Digital MS-2/6, Ismatec, USA) at $\dot{V}_{Susp} = 7.0$ mL/min. Flow rate of air was 2.8 mL/min.

Commercial ASA (ASS3020, GL Pharma, Austria) was used as a model substance in all experiments. By sieving the received rodlike crystals of ASA (sieve fraction between 90 and 200 μm), crystals with a maximum Ferret diameter (f_{max}) of 500−1000 μm were separated and subsequently suspended in a saturated aqueous solution, i.e., the starting suspension. The starting suspension was continuously stirred at 22 °C at sufficient speed to simultaneously prevent sedimentation and to avoid breakage of the crystals (stir bar: 4×0.5 cm, 500 rpm). To study the influence of the solvent's polarity on the resulting shape, three different solvents were selected: (1) 1-hexanol (≥98%, Carl Roth GmbH, Germany), (2) 2-propanol (isopropanol, laboratory reagent grade, Fisher Scientific GmbH, Austria), and (3) ethanol (≥99.8% denatured, Carl Roth GmbH, Germany). The chemical and physical properties of the used solvents are listed in Table 1. In these solvents, ASA shows a solubility decreasing from ethanol to hexanol with increasing length of the hydrocarbon backbone and decreasing polarity.

For online product analysis, a QICPIC automated microscope (pixel size = 19.63 μm, software version: WINDOX 5.6.0.0, Sympatec, GmbH, Germany) was installed, equipped with a flow cell (LIXELL, optical path length = 2 mm, diameter of window = 33 mm, Sympatec
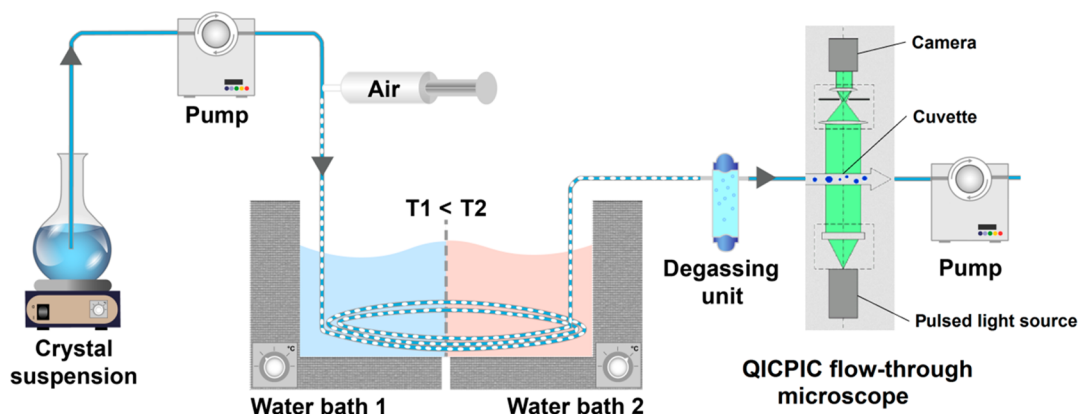

Figure 2. Setup of the tubular crystallizer.

Table 1. Properties (Boiling Point, Density, Viscosity, and Dielectric Constant) of Pure Solvents at Room Temperature

solvent	T_s [°C]	ρ [kg/L]	μ [mPas]	ε [-]
ethanol	78	0.789	1.2	25
isopropanol	82	0.78	2.2	18
hexanol	157	0.81	5.9	13

GmbH, Germany). At the outlet of the tubular temperature cycler, a stirred 50 mL round-bottom flask kept at 22 °C via a thermostatic bath beaker was installed for degassing. Whenever 35 mL of product suspension was collected in the beaker, it was pumped at a higher flow rate of 90 mL/min through the QICPIC system, which recorded videos at 450 fps (measurement duration: 20 s each, range of size: 20−6820 μm). The videos were analyzed using an in-house Matlab routine as described below.

Figure 3 shows details of single frames from the videos taken by Sympatec's QICPIC, which were the basis for all further analysis.

2.2. Process Settings. During the first set of experiments, the change of crystal shape after 5, 10, 15, and 20 cycles was investigated using ethanol as a solvent and compared to the results after 25 cycles. The second set of experiments were focused on crystal-shape tuning via temperature cycling utilizing three different solvents, i.e., ethanol, isopropanol, and hexanol. In order to easily compare results, the temperatures in the water baths were chosen such that, for all solvents, the same maximum under- and supersaturation of S_{min} = 0.89 and S_{max} = 1.23 were achieved. The supersaturation S is defined as the ratio of concentration and true solubility $S = c/c^*$.

Due to the different solubility for each solvent, the amount of dissolved material (solute) available for deposition during crystal growth varies, dependent on the solvent. To compensate for this effect, the ratio of $m_{seeds}/m_{ASA\ dissolved}$ was kept constant at 1% for all solvents used. Thereby, the concentration of seeds in the starting suspension was low enough to minimize aggregation of the particles and, in addition, did not exceed the critical optical density for QICPIC measurements. Due to the small amount of seeds and the short residence times in each water bath, the solution concentration (as a means for calculation of the super- and undersaturation) was

considered constant along the tubular crystallizer. The settings for each experiment are summarized in Table 2. Solubility data of ASA were either taken from the literature (ethanol and isopropanol)[41] or determined via density measurements (hexanol; see the Supporting Information (SI)).

In a recent study,[40] we reported on a computational approach to model the temperature profile in the tubular reactor during heating and cooling. For the present study, in combination with the solubility data of ASA in ethanol,[41] isopropanol,[41] and hexanol (see the SI), the supersaturation profiles along the temperature cycler were calculated in an appropriate way. Results of these calculations supported the determination of temperatures in the water baths to minimize net changes in crystal volume after each cycle; i.e., dissolved crystal mass in the warm water bath should be compensated by regrowth in the cold water bath (see Figure 4).

During the cycling process, the crystal's surface roughness and the relative exposure of different crystal faces vary. Therefore, face-specific perpendicular growth rates are nonconstant and an exact prediction of crystal size behavior is not feasible. Accordingly, suitable levels of under- and supersaturation were determined via preliminary experiments using isopropanol as follows: For the cold water bath, its lowest temperature was given by the metastable limit of ASA, since nucleation should be excluded in all experiments. In the warm water bath, complete dissolution of the crystals had to be avoided. Isopropanol was chosen for these preliminary experiments, showing a polarity between the one of ethanol and hexanol as it allowed drawing presumptions on the behavior of both of the other solvents.

As can be seen in Figure 4, the temperature and supersaturation change along the tubular crystallizer in a periodic manner. Despite the high heat-transfer rates, the respective bath temperatures are only (asymptotically) reached at the end of each segment, and thus, for most of the crystallizer, there is a transient change of supersaturation.

2.3. Image Analysis. Static image analysis, i.e., the standard postprocessing procedure, is generally performed offline, after a process of sampling, drying, and dispersion, which possibly leads to some degree of particle change (e.g., via attrition) and, thus, to biased results. Furthermore, only a small fraction of the entire crystal population can be observed. The QICPIC system collects 2D videos of particles at a rate of 450 frames per second (fps) as they pass through the LIXELL flow cell. Using this setup, particles are not
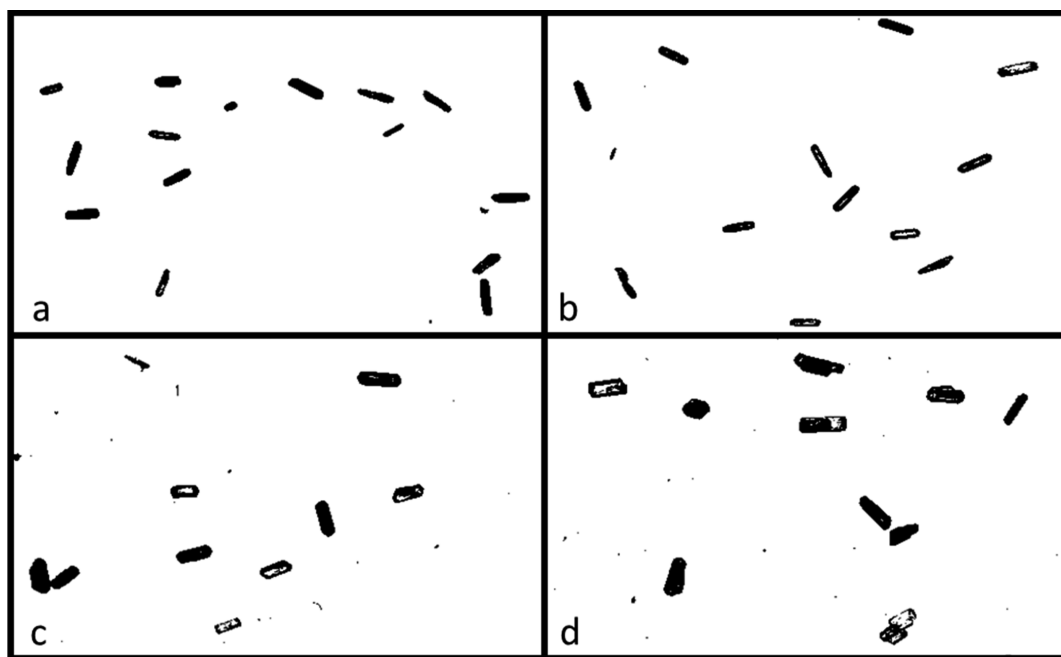

Figure 3. Details of single nonconsecutive frames captured by QICPIC, showing (a) the seed crystals, (b) product in hexanol, (c) product in isopropanol, and (d) product in ethanol.

Table 2. Experimental Settings Used for the First Set of Experiments[a]

solvent	$c*$ (22 °C) [g/100 g solv.]	T (water baths) warm/cold [°C]	S_{max}	S_{min}	amount of seeds [g seeds/100 g sat. sol.]	$m_{seeds}/m_{ASA\ dissolved}$ [%]
ethanol 99.8%	22.6	25.0/17.0	1.23	0.89	0.189	1
isopropanol	11.6	23.9/19.0	1.23	0.89	0.107	1
hexanol	5.4	24.3/18.6	1.23	0.89	0.053	1

[a]That is, varying the solvent but keeping equal levels of supersaturation during temperature cycling. $c*$ (22 °C) = solubility of ASA in the respective solvent at the temperature of the starting suspension.
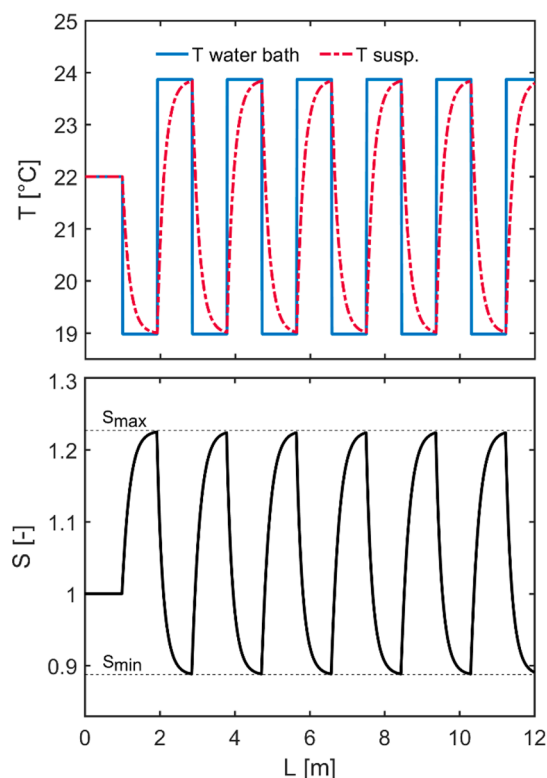

Figure 4. Modeled temperature (top) and supersaturation (bottom) profile of ASA using isopropanol as solvent during the first six temperature cycles.
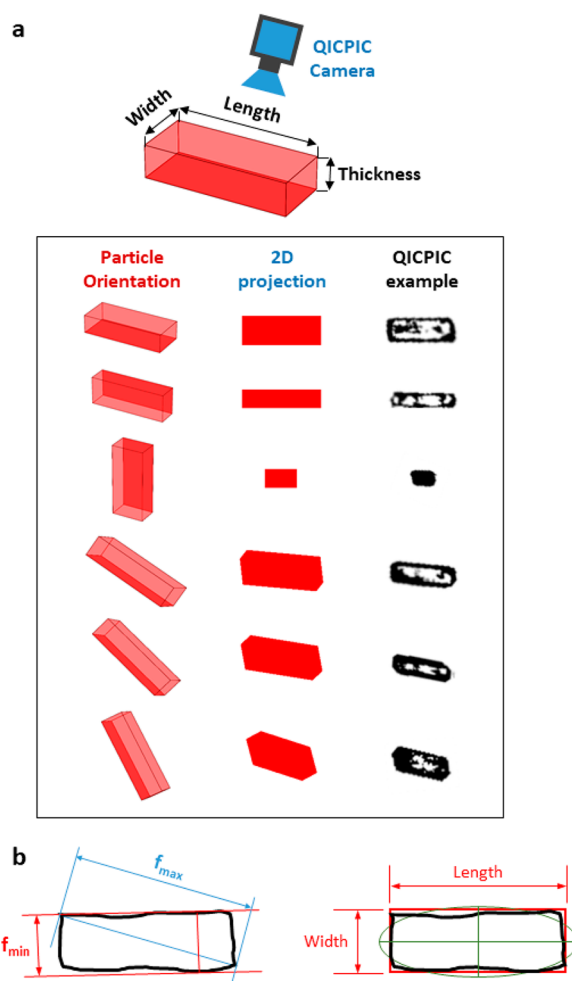

Figure 5. (a) Illustration of multiple projections of the same particle depending on the orientation with respect to the plane of inspection of the camera, which is fixed at the top. One of the faces of the cuboid is shaded for easier visualization of the particle's rotation. Using particle tracking, a single set of size characteristics is taken from all the projections observed. (b) Scheme of the particle sizing algorithm utilizing length and width (right) instead of f_{min} and f_{max} (left) to measure the aspect ratio. The thickness is defined as the smallest width among all the projections of every individual particle.

exposed to mechanical stress. Moreover, the entire population is analyzed, and consequently, the results are more representative. Finally, within a flow cell, particles revolve as they transit through the field of view of the camera and are observed from many different directions, while static image analysis "sees" only the lowest energy orientation. Out-of-plane dimensions cannot be analyzed with standard microscopes.

Sympatec's QICPIC software offers a frame-by-frame identification of particles. However, concerning shape analysis of particles, it has three major drawbacks: (I) Since particle velocities in the flow cell are not constant (laminar velocity profile), particles that move slower are "seen" more often and, therefore, have a more significant contribution toward the final size and shape distributions. (II) During the passage of a single particle through the flow cell's field of view, it is captured by the camera on several consecutive frames. Its revolving motion in the liquid stream and QICPIC's frame-by-frame identification of particles result in multiple records and, hence, multiple sets of size characteristics for each particle, as illustrated in Figure 5a. The particle's dimensions and the true size of the major face, which can only be identified from the projection with its principal axis of inertia parallel to the line of inspection, are hereby generally underestimated. (III) The software analyzes the maximum and minimum Feret diameters (f_{max} and f_{min}) of each particle in each frame to calculate its aspect ratio. Although similar approaches have also been used to estimate particle shape distributions from inline imaging probes,[42] for

the analysis of single faces of faceted crystals, using f_{min}/f_{max} of the crystal as aspect ratio is inadequate. As shown in Figure 5b, f_{max} correlates with the space diagonal of the particle, being substantially longer than the length of the largest crystal face. Depending on the respective projection, f_{min} will range from the thickness of the particle to its width, generally underestimating the aspect ratio of the largest face.

Therefore, the recorded sequences of images taken from QICPIC's video were analyzed via an in-house Matlab routine. The main improvements over standard image-processing algorithms are (I) the introduction of a particle tracking mechanism, (II) the evaluation of

particle length and width using an appropriately oriented bounding box, resulting in more accurate sizing, (III) the identification of the particle's thickness, and (IV) the implementation of a solidity filter to discard aggregates.

The ability to record a large number of images from different angles for each particle is a major advantage. However, not all the views are relevant for particle sizing purposes and it is important to yield only one single set of size and shape characteristics for every given particle. Therefore, our image analysis algorithm incorporates a particle tracking mechanism by which objects are followed across consecutive frames until they leave the field of vision. This allows many images of a particle to be assigned to that individual particle. The Motion-based Multi Object Tracking module[43] from Matlab's Computer Vision System Toolbox was used as the basis for the particle tracking algorithm, although some modifications were introduced. In order to ensure that every crystal is well characterized, only objects that have been detected in N_{views} or more consecutive frames are included in the analysis. The value of the minimum number of views N_{views} is experimentally evaluated in the present work. Particles colliding or overlapping in the flow cell were removed from the analysis based on abrupt changes in particle size. Using trajectory prediction, overlapping particles are reassigned to their original track after diverging.

In the present work, crystal habits range from rod-shaped to elongated cuboids and platelike sheets. In order to make crystal dimensions comparable, all crystals were assumed to be cuboids, differing in length (longest dimension of the cuboid), width (second longest dimension), and thickness (shortest dimension), as shown in Figure 5a. However, the individual frames collected by the QICPIC instrument only contain 2D projections of the original three-dimensional particles. Generally, image analysis algorithms extract particle size and shape characteristics from these projections. A visual comparison of Sympatec's software particle sizing method and our approach is given in Figure 5b. In contrast to the original determination of the particle size via f_{max} and f_{min}, the dimensions of the particles are established through appropriately oriented bounding boxes. The *regionprops* function[44] from Matlab was used as an intermediary to establish the dimensions of each individual projection. The function operates through ellipse fitting, by which the center, size, and orientation of an ellipse are optimized in order to achieve the representation that has the closest second moments as the particle (see Figure 5b). The length of the major and minor axes of the ellipse could be used as a measure of particle length and width. However, these axes are generally longer than the particle itself, as seen in Figure 5b. Instead, a bounding box around the particle with the same orientation as the ellipse is a more accurate representation. The length and width of the particles used in the present work correspond to the sides of this bounding box. The aspect ratio of the particle is calculated as the ratio of its width and its length. These size and shape characteristics of each particle are extracted from the projection with the largest area among the different views of this particle as it is tracked across several frames. This projection is more likely to correspond to the view of the particle with its central principal axis of inertia parallel to the line of inspection. Therefore, the resulting length and width will be the best representation of the actual particle's dimensions in the set of size characteristics from the 2D projections. The area of the different projections can be determined by counting the number of pixels that form these objects and by then applying the corresponding transformation into physical dimensions using the known pixel size (i.e., 19.63 μm/pixel). Other approaches for particle characterization are also available and emphasize the importance of the use of multidimensional particle size analysis in crystallization processes. Previous studies[45−47] assume a number of different particle shapes (i.e., spheres, cylinders, needles, and cuboids with flat or pyramidal faces) and suggest additional descriptors based on the distance from the centroid to the boundary of the particles. Although more accurate contours can be obtained through these methods, this level of detail is not required in this work since the suggested particle characterization in terms of the properties of a cuboid (see Figure 5a) is accurate enough for the purpose of this work.

Using our particle tracking approach, not only the true size of the particle in terms of its length and width becomes accessible but also its thickness can be determined, being the smallest width found among the different projections observed for that particle. However, due to the measuring principle, the identification of the particle's thickness is most sensitive to capturing the projection aligned with the thickness facet, particularly in the case of platelike particles, as is the case in this work. For crystals for which width and thickness are significantly different, the ratio of thickness to width—denominated T/W ratio in this work—is a good indicator of the level of rotation of the particles. Values close to unity would imply that the particles do not revolve significantly and the same face is continuously exposed to the camera.

Another important feature incorporated in the algorithm is a solidity filter. The solidity of an object is defined as the ratio of the area of an object to the area of its convex hull. Typically, individual ASA crystals are not concave. Therefore, low solidity indicates the presence of concave parts of a structure, i.e., being a sign for particle aggregation or overlap. Previous studies[48,49] have used solidity filters to classify the particles in terms of their level of aggregation. According to those studies, the solidity threshold above which an absence of aggregation is assumed varies from 0.85 (combined with a minimum circularity of 0.5) to 0.95. More complex schemes based on machine learning algorithms such as discriminant factorial analysis[46] have also been suggested for the treatment of aggregates but require the generation of a sufficiently large training set. In our work, data availability is not large enough to obtain accurate results through this method. Therefore, it was decided to discard any object with a solidity lower than 0.9, which provided adequate filtering as confirmed by visual inspection of the discarded objects.

Finally, to avoid the influence of fines on the results, only objects with an area larger than 50 square pixels (length of 138.8 μm for objects of aspect ratio 1) are considered in the analysis. A filter is also applied to objects larger than 1600 square pixels (length of 785.2 μm for objects of aspect ratio 1) to be sure that aggregates are not considered in the analysis.

3. RESULTS AND DISCUSSION

This section presents the results obtained in this work. First, the importance of the particle tracking and aggregate rejection features included in our image analysis algorithm is demonstrated. Then, the influence of the number of cycles of growth and dissolution and the nature of the solvent on the particle size and shape distributions of the final product is analyzed. To ensure that the measured size and shape distributions are statistically representative, the analysis requires a minimum population of 500 particles.[50,51] Moreover, the reported distributions are the result of averaging three independent cycling experiments. The standard deviations of these averages are shown as error bars in the respective figures.

3.1. Importance of Particle Tracking and Aggregate Rejection. The high image acquisition rates of the QICPIC instrument provide the opportunity to observe several views of every individual particle as they transit through the flow cell. However, different particles move at different velocities depending on their position within the flow cell and their alignment with respect to the direction of the flow. Therefore, the slower particles are observed at more occasions and have a larger contribution toward size and shape distributions. In addition, the dimensions of the particles are only representative when the appropriate crystal face aligns with the camera inspection plane. Any tilt of the particle will result in views that might not correspond to an actual crystal face. Including the size and shape of these elements in the analysis also alters the final size and shape distributions. Particle tracking avoids these statistical biases by reducing the contribution of each particle
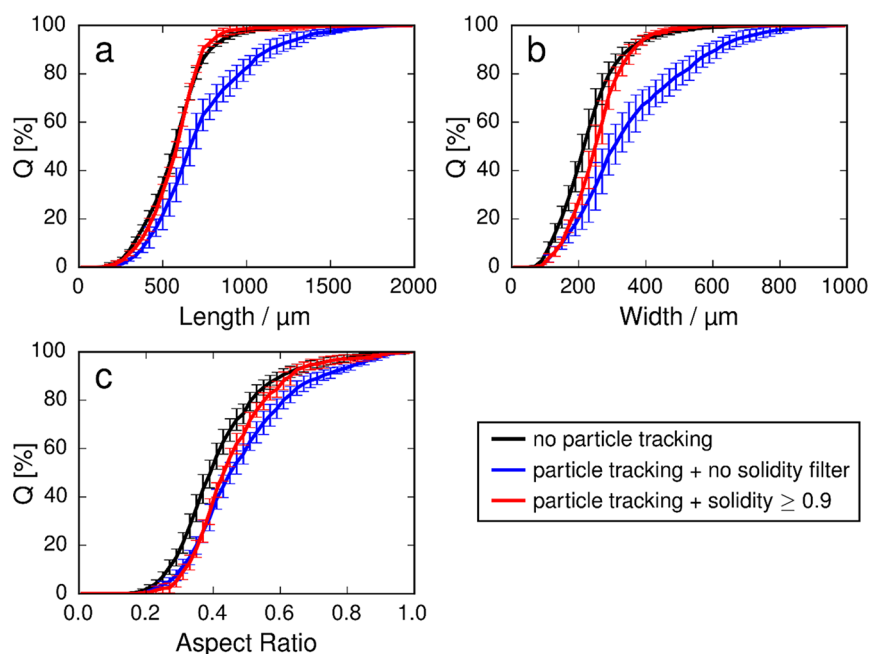
Figure 6. Influence of the implementation of particle tracking and solidity filter on the number-based cumulative distribution of (a) length, (b) width, and (c) aspect ratio in shape tuning experiments of ASA in isopropanol after 25 cycles.
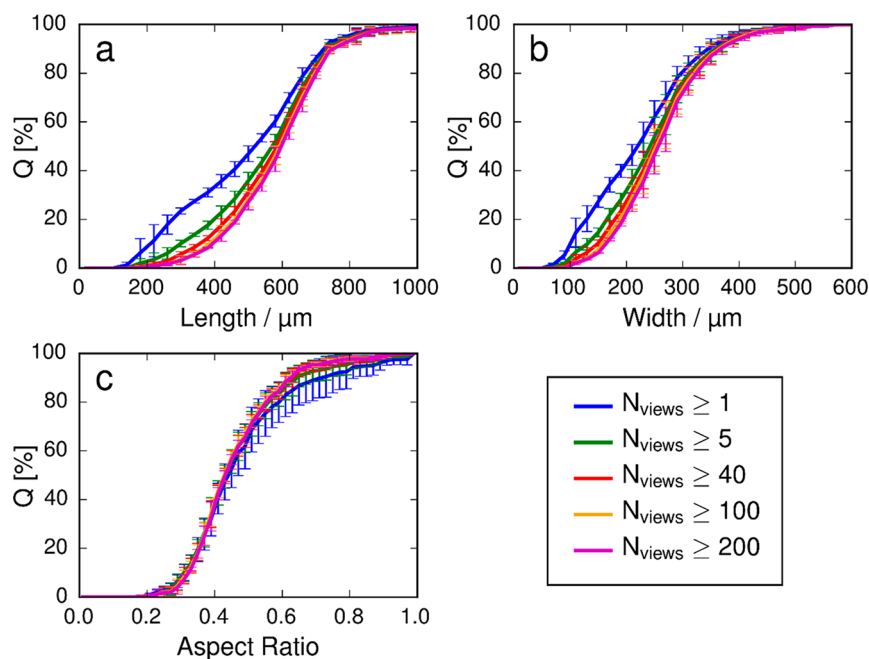

Figure 7. Influence of the minimum number of views of each individual particle on the number-based cumulative distribution (including the solidity filter) of (a) length, (b) width, and (c) aspect ratio in shape tuning experiments of ASA in isopropanol after 25 cycles.

to a single set of features representing its true dimensions, allowing a more accurate characterization of the crystals. Figure 6 shows the influence of the particle tracking algorithm on the (a) length and (b) width number-based cumulative distributions of ASA in isopropanol, as well as on the (c) aspect ratio distribution, where the aspect ratio of each particle is defined as the ratio of its width and length.

The raw size distributions (black lines), which include all recorded views of each particle, shift to larger sizes when particle tracking is applied (blue lines). This is a consequence of discarding the length and width of tilted and smaller

projections of the particle that do not correspond to the major crystal face. Similarly, the aspect ratio distribution also shifts to larger values since the effect of particle tracking on the particle width distribution is more significant than that on the particle length distribution.

Depending on the revolving speed of the particles as they pass through the flow cell, the more views are recorded for each particle, the more representative the measured dimensions of the particles will be since the alignment of the crystal's faces with the camera inspection plane will be more probable. In order to ensure the representability of the results,

particles that are being tracked in only a minor number of frames are excluded from the analysis. Figure 7 shows how a distinct shift toward larger lengths and widths is observed as the minimum number of views required for each particle is increased. This shift continues until only particles with a minimum of 40 views (i.e., 40 pictures of the same particle in different orientations as it passes through the flow cell) are considered in the evaluation. Increasing the minimum number of views after this point does not yield a statistically significant change in length and width. Although the effect on the aspect ratio distribution is not critical (see Figure 7c), using only objects with at least 40 views ensured both a reliable measurement of the particles' dimensions and a minimum of 500 objects detected in each of our experiments.

Finally, aggregates of crystals and overlaps occurring during the particle's motion through the flow cell introduce a bias in particle size and shape measurements. As mentioned previously in section 2.3, a solidity filter is incorporated in the image analysis algorithm to treat this issue. Figure 8 shows
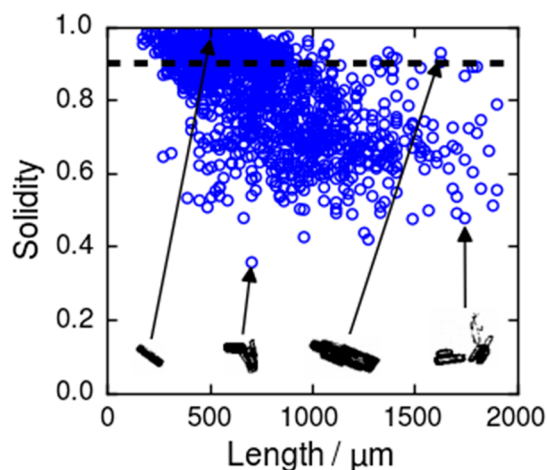

Figure 8. Scatter plot of solidity vs length for product ASA crystals after 25 cycles in isopropanol. The black dashed line corresponds to the solidity threshold applied in our analysis for the rejection of agglomerates and overlaps.

the distribution of solidity and length for all the particles detected in a shape tuning experiment of ASA in isopropanol. For individual particles, the solidity approaches the value of 1, while aggregates and overlaps, which generally present concavities, tend to have lower solidities. Effective implementation of a solidity filter with a threshold at solidity values of 0.9 allowed for discarding of these objects. When isopropanol was used as a solvent, 55% of the detected particles have been rejected by the solidity filter, emphasizing the importance of this processing step. The percentage of aggregate rejection varies from 54% for the seed crystals to 47% and 70% after 25 cycles of growth and dissolution in hexanol and ethanol, respectively. As shown in Figure 8, the rejected particles tend to have larger sizes than those accepted by the filter. As a consequence, the length and width distributions narrow down toward smaller and more representative sizes (shown as red lines in Figure 6a,b). The aspect ratio distribution also shifts to lower values than that corresponding to the simple application of particle tracking (see Figure 6c). However, it still shows a significant increase with respect to the original results without particle tracking.

Both the particle tracking mechanism as well as the solidity filter included in our algorithm have a significant influence on the particle size and aspect ratio distributions. This approach is applied to the results presented below since it provides the best representation of the crystal population.

3.2. Shape and Volume Changes of Crystals after Different Numbers of Cycles. The change of crystal shape of ASA crystals by temperature cycling in ethanol was investigated using an increasing number of cycles of growth and dissolution. Generally, during growth, crystals evolve toward a steady-state shape, which is in contrast to dissolution.[22] Thus, during cycles of growth and dissolution, crystals do not asymptotically evolve toward a steady-state shape but rather show a continuous change in shape.

Accordingly, due to the higher relative perpendicular growth rate of the (001) face compared to the (100) face, from the rodlike starting material, a single major face, being the (100) face, appears. The measured aspect ratio will reach a maximum when this (100) face becomes a square. If the cycling proceeds, the width will become the longest dimension of the crystal and the aspect ratio will decrease again.

The results of our experiments varying the number of cycles between 5 and 25 are summarized in Figure 9 as number-based cumulative distributions of size, aspect ratio, and thickness-to-width (T/W) ratio. While the length and width grow considerably with respect to the original ASA seeds after 25 cycles, during the initial ~5−10 cycles, the length exhibits a distinct decrease and the width is not greatly affected, as shown in Figure 9a,b, respectively. SEM images (Figure 10a) illustrate a high surface roughness on all sides of the seed crystals. This could induce an accelerated dissolution rate during the first cycles on the one hand due to increased effective surface area. On the other hand, strain and defects at the surface have shown to reduce the crystal's growth rates.[52,53] Both effects could be contributing to the observed behavior.

Following the overall shrinkage of the crystals, the results show strong increase of both the length and width after 15 cycles, corresponding to an anticipated overall increase in crystal volume for cycling in ethanol under the present conditions. The smooth surface of the crystals faces after this number of cycles, visualized by SEM in Figure 10b for the major (100) face, is assumed to be responsible for the decrease in overall dissolution rate. Both the initial decrease in particle length for the first 5−10 cycles and the overall growth of the particle after 15−20 cycles (with a larger relative growth of particle width) result in an increase of aspect ratio, as shown in Figure 9d. As discussed in section 1, this effect can be substantiated with the polarity of the solvent, resulting in favorable interaction with the (001) face and its hydrophilic nature.

The sample QICPIC images in Figure 9d show a clear transition from the rodlike seeds to platelike crystals after 20−25 cycles, confirmed by the SEM images in Figure 10. Despite an initial decrease after 5 cycles, the particle thickness does not seem to be significantly affected by the consecutive cycles of growth and dissolution during the initial 20 cycles (see Figure 9c). However, a noticeable increase is observed after 25 cycles. It is possible that, after an initial increase of the particle's width, further growth occurs in the direction perpendicular to the (100) face, leading to larger particle thickness. The results shown in Figure 9e for the evolution of the T/W ratio with increasing number of cycles illustrate this hypothesis. Initially, the larger growth of the particle width with respect to its
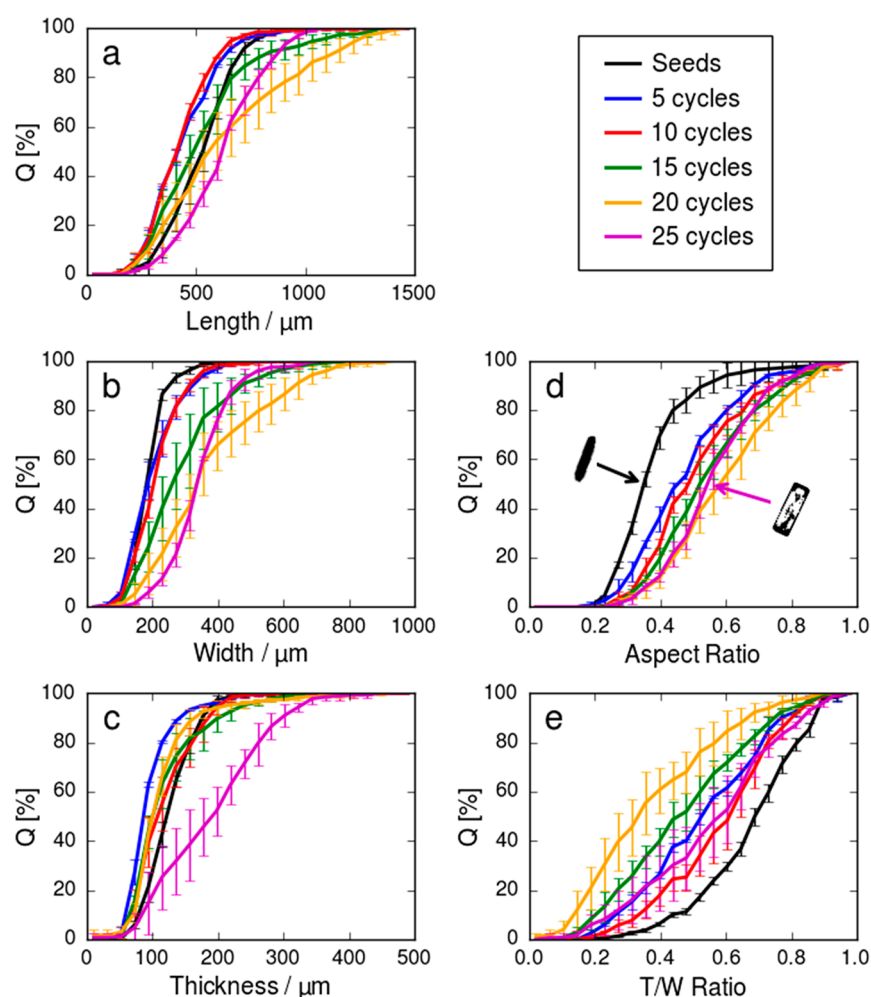
Figure 9. Influence of the number of cycles of growth and dissolution on the number-based cumulative distribution of (a) length, (b) width, (c) thickness, (d) aspect ratio, and (e) T/W ratio of ASA crystals suspended in ethanol.
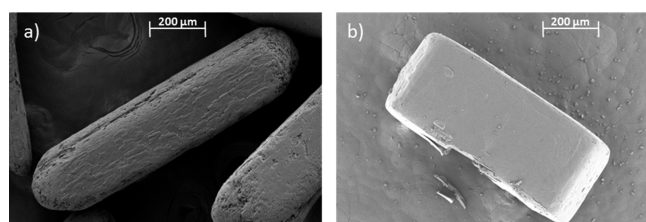

Figure 10. SEM images of (a) seed and (b) product crystal (after 25 cycles in ethanol). SEM: Zeiss Ultra 55, Zeiss, Oberkochen, Germany operated at 5 kV. Sputtering of particles with gold-palladium prior to analysis.

thickness, which even shrinks during the first 20 cycles, yields a decrease of the T/W ratio. After 25 cycles, the particles tend to grow in thickness rather than in width, which results in an increase of the T/W ratio. However, the same effect would be observed if the rotation of the crystals within the LIXELL flow cell was somehow hindered and the thickness face was not accessible to the camera. The platelike crystals formed after 25 cycles are more prone to a certain alignment with the flow than the initial rodlike particles whose rotation is less impeded. The introduction of static mixers to promote turbulence within the flow could be a possible solution to discard particle alignment and confirm the results obtained after 25 cycles of growth and dissolution.

3.3. Solvent-Influenced Shape Tuning. This section shows the results obtained for shape tuning experiments of ASA carried out in three different solvents (hexanol, isopropanol, and ethanol). During these experiments, the suspensions underwent a total of 25 cycles of growth and dissolution between $S_{max} = 1.23$ and $S_{min} = 0.89$. The effect of the properties of the solvent on the final size and shape distributions of the product was studied by comparing the cycled crystals to the seeds. According to the shape of the seed material and the shape evolution during different numbers of cycles, changes in particle length are associated with the (110) face and net growth or dissolution on the (001) are associated with the crystal's width.

The polarity of the solvent has a significant influence on the final product crystal's shapes. In order to ascribe resulting shapes after temperature cycling (considering the (100), (001), and (110) faces) to the respective solvent (and its polarity), other effects on crystal shape had to be minimized. On the one hand, during the dissolution steps, the complete disappearance of one of the three groups of faces of interest was avoided by short residence times in each of the water baths. On the other hand, we assumed that growth on faces appearing on the crystal surface during dissolution by bifurcating from edges and vertices is much faster than on the faces of interest, ensuring their rapid disappearance during regrowth. Also, if the same relative rates of growth and
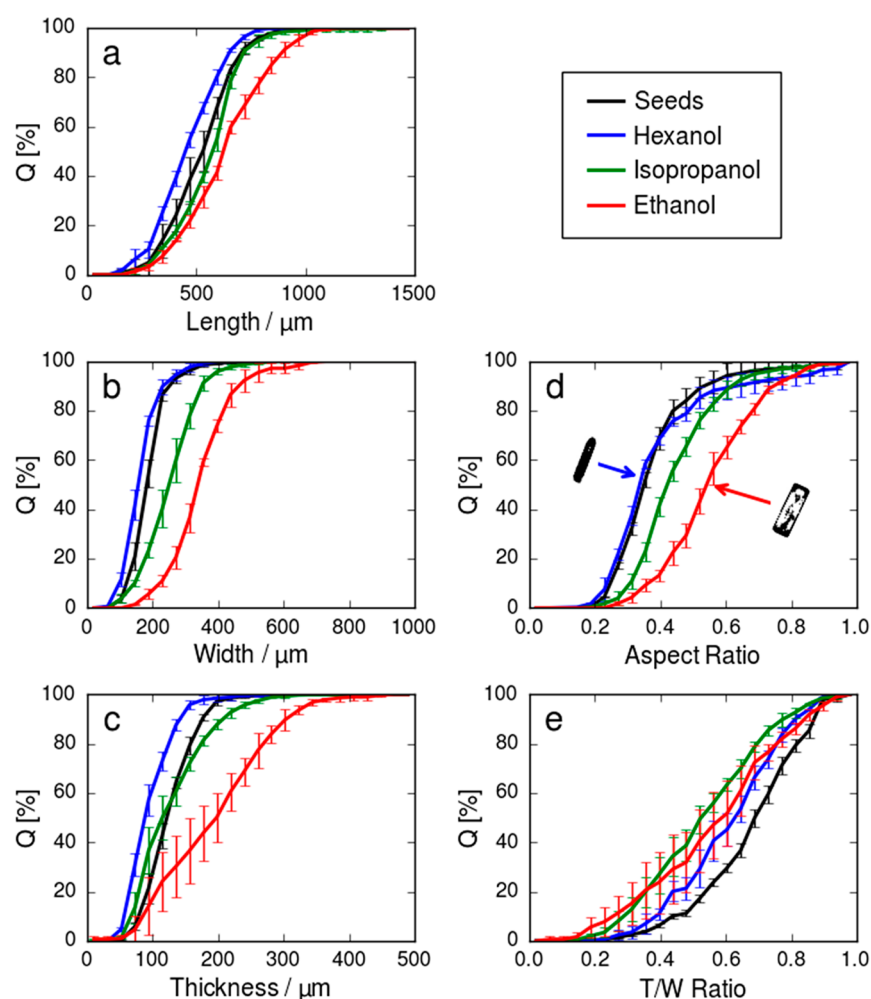
Figure 11. Influence of solvent-influenced shape tuning on the number-based cumulative distributions of (a) length, (b) width, (c) thickness, (d) aspect ratio, and (e) T/W ratio of ASA in different solvents.
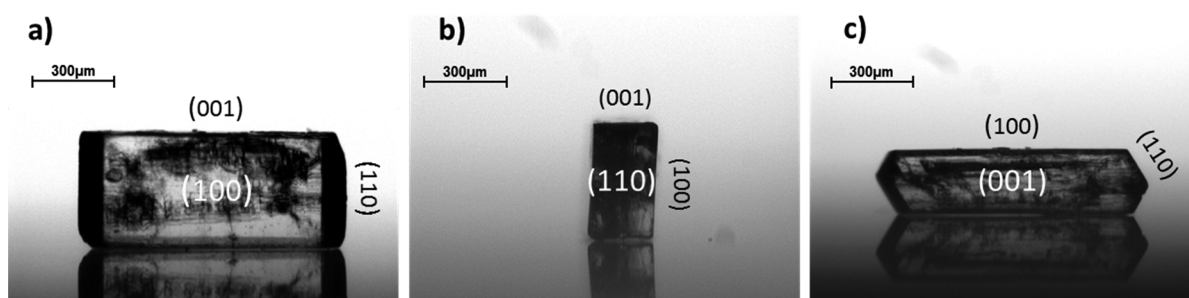

Figure 12. Horizontally taken microscope images of a single product crystal (length = 975 μm, width = 415 μm, and thickness = 240 μm) temperature cycled in ethanol. The crystal is photographed with its principal axes of inertia parallel to the line of inspection, showing (a) its (100) face, (b) its (110) faces, and (c) its (001) face. Neighboring faces are indicated in black font. The faces could be assigned to their respective indices according to the relative position of the sloped (110) face.

dissolution were present for each face, the final product would differ in the overall volume but each face would experience proportional growth maintaining its shape.

Figure 11 shows the results of the cycling experiments using the three different solvents (see Table 1 for their properties). As can be seen in Figure 11a,b, for the polar solvent ethanol, both the length and width shift to larger sizes relative to the seed material. In addition, the aspect ratio distribution in Figure 11d shows a distinct shift to the right. This is equivalent to a larger relative increase in width, resulting from a major

(100) face appearing after cycling the rodlike seeds in ethanol, as discussed in section 3.2. Microscope images of a single product crystal were taken from three different angles (see Figure 12) and compared to the growth morphology of ASA (see Figure 1). Thus, the major face formed when cycling in ethanol was identified to be the (100) face.

Similar to ethanol, also for isopropanol, a transformation to a platelike habit was observed. The shift of the aspect ratio to the right is less pronounced and the length and width show less relative growth. This indicates that, for both faces (i.e., the

(110) face determining the length and the (001) face determining the width), the perpendicular growth rates are less increased relative to their respective dissolution rates compared to ethanol. As the effect is still more pronounced for the (001) face, crystals evolve toward a platelike shape. In contrast, for hexanol (the least polar solvent), the width, as well as the length, of the crystals decreases. This exhibits rates of growth being smaller than rates of dissolution for all three types of faces under the conditions chosen in this study. The (001) face shows a slightly more pronounced deceleration of the perpendicular growth rate, and therefore, crystals eventually tend to transform into more needle-like shapes. Therefore, the polarity of the solvent has a clear influence on the shape of ASA crystals, as observed in the QICPIC sample images in Figure 11d and substantiated by molecular dynamic simulations[28] (see section 1).

Assuming cuboid-like particles, their volume can be calculated via the product of length, width, and thickness of the crystals. The accuracy, though, is limited by the number of different views captured by the camera for each particle, i.e., the different orientations accessible to the analysis. The more platelike the crystals are, the more the calculation of the actual thickness and hence the volume depends on capturing the particle's smallest dimension which becomes less likely to be observed. According to the results presented in Figure 11c, the thickness of ASA particles suspended in hexanol decreases with respect to the original seeds after 25 cycles of growth and dissolution. The initial smoothing of the seeds observed during the first cycles when ethanol is used as a solvent, which translates in a reduction of particle thickness (see Figure 9c), might occur similarly in hexanol. However, this phenomenon is not followed by growth rates higher than dissolution rates, as it was the case in ethanol, due to the less polar nature of hexanol. Therefore, the particles tend to shrink with respect to the original seeds. The results obtained using isopropanol as a solvent show again an intermediate behavior. After 25 cycles, the process in isopropanol appears to be in a phase where the relative growth on the (001) face is still more intense than the one on the (100) face, as suggested by the low T/W ratios observed in Figure 11e.

Concerning crystal volume distributions, results from our experiments show significant deviations of the product crystal with respect to the seeds, as observed in Figure 13. It is noted that the proposed approach can accurately estimate the width and the length of the crystals. However, thickness measure-
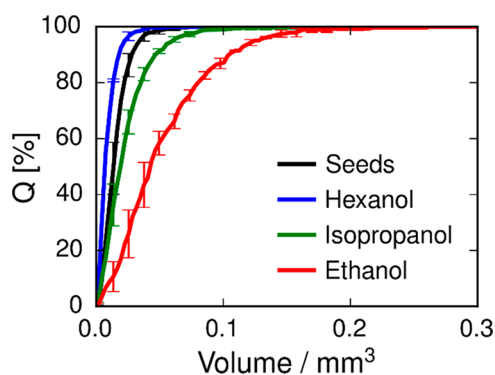
ments are more sensitive to the angle of inspection and may impact the absolute measurement of volume. Nevertheless, the volume shifts can in part be explained by the effect of the solvents polarity-dependent growth rates and are in line with results obtained in molecular dynamics simulations:[28] In nonpolar solvents, transition into a more needle-like shape is caused by, decelerated (re)growth at the (001) surface rather than by accelerated growth at the (110) surface. Therefore, the overall volumetric growth rate of the crystals is expected to be smaller the less polar the solvent is. As dissolution rates are comparatively less affected by the solvent's polarity, imposing the same saturation trajectory for all solvents used in this study leads to different mean product crystal volumes. Although the individual product crystal's volume might not be equal to the volume of its seed, the resulting crystal shape (in terms of the ratio of length:width:thickness) is likely directly related to the used solvent.

It can be concluded that, as expected, in each solvent, multiple faces of ASA show varying relative rates of growth and dissolution, offering a method to achieve target crystal habits that are not accessible by growth alone. According to our results, particularly the (001) face is affected by the solvent polarity. Cycling in more polar solvents enhances growth on the (001) face in relation to its dissolution. Using rodlike seeds, this leads to an increase in particle's width. By using a less polar solvent (such as hexanol), the perpendicular growth on the (001) face can be minimized, resulting in a slow evolution toward a needle-like shape.

4. SUMMARY

In the present study, a unique setup for rapidly altering saturation levels was developed. The system was shown to be able to change the shape of crystals via cycles of growth and dissolution. While the solvent factor is generally less important on dissolution of crystal faces, it has a strong impact on the face-specific incorporation of molecules during growth. Therefore, due to the (001) face of ASA crystals being most affected by the polarity, changes in crystal shape could be achieved using three different solvents.

While theoretical approaches and simulations of crystal shape changes via cycles of growth and dissolution deal with single particles, the present experimental work deals with distributions of sizes and shapes as are present in real-life manufacturing settings. Non-uniform starting material exhibiting differences in the presence and relative exposure of faces might cause a relevant variation in the product crystal shape. Particularly, for the dissolution rate, the volume and the specific surface area of the individual particles of a population are critical. While, for one crystal, a certain face might disappear completely (therefore becoming a virtual face), it is still present on the surface of another one. During regrowth, real and virtual faces show different perpendicular growth rates, resulting in broadening of the shape distribution.

We showed that rapid temperature cycling in different solvents can be a valuable mechanism for generating crystal shapes that are not obtainable through either growth or dissolution alone. By understanding the interplay between the face-specific functional groups and the solvents properties and its effect on the relative rates of growth and dissolution of single faces, the crystal shape can be tailored.

Our results together with theoretical considerations suggest that, by employing different solvents successively, virtually any

Figure 13. Number-based cumulative distribution of crystal volume V calculated via $V = length \times width \times thickness$ for seed crystals and for product crystals after temperature cycling in different solvents.

convex shape for faceted crystals is attainable via temperature cycling.

Due to their superior heat-transfer properties, tubular crystallizers are well suited for particle engineering, owing to the ability to rapidly change the temperature, a field of applications where conventional batch crystallizers quickly reach their operational limits.

While some of the resulting crystal shapes of ASA crystals obtained during this study might not reflect the typical requirements from industry concerning powder handling (e.g., flowability, filtration, capsule filling, tableting, and further downstream processes), particles with increased specific surface area as is typical for platelike crystals might be interesting for fast dissolution dosage forms. Furthermore, the presented setup can easily be adapted for other crystallization systems.

Based on an automated microscope, in the present study, a particle imaging technique was established that allows assigning a large number of different projections to each single particle via particle tracking. Besides 2D characteristics, such as length and width, using our dedicated analysis routine facilitates the determination of the particle thickness and the associated derivative parameters, such as particle volume, sphericity, and solidity, although its application is limited in the case of platelike crystals as the analysis is highly sensitive on capturing the required projection. Improvement of our method could be achieved via increasing the fluid recirculation in the flow cell, enhancing the ability to take images with a higher number of orientations/projections. A static mixer installed at the entrance of the flow cell could increase the mixing, leading to enhanced revolving of the particles. This is promising regarding the identification of the true 3D habit of irregularly formed particles.

Furthermore, our setup could be used to change crystal shape by altering the saturation trajectory alone. However, experiments with this goal have shown that differences in the saturation trajectory large enough to achieve different relative rates are not feasible for ASA, due to limitations concerning the nucleation in the cold water bath and complete dissolution in the warm water bath.

ASSOCIATED CONTENT

S Supporting Information

The Supporting Information is available free of charge on the ACS Publications website at DOI: 10.1021/acs.cgd.8b00371.

Determination of the solubility of acetylsalicylic acid in hexanol via density measurements (PDF)

AUTHOR INFORMATION

Corresponding Author

*Tel.: +43 316 873 30400. Fax: +43 316 873 1030400. E-mail: khinast@tugraz.at. Web: ippt.tugraz.at and www.rcpe.at.

ORCID

Peter Neugebauer: 0000-0002-9671-9997
Javier Cardona: 0000-0002-9284-1899
Maximilian O. Besenhard: 0000-0002-5079-617X
Heidrun Gruber-Woelfler: 0000-0002-6917-4442
Johannes G. Khinast: 0000-0002-2076-1822

Notes

The authors declare no competing financial interest.

REFERENCES

(1) Law, M.; Greene, L. E.; Johnson, J. C.; Saykally, R.; Yang, P. Nanowire dye-sensitized solar cells. *Nat. Mater.* **2005**, *4*, 455−459.

(2) Heng, J. Y. Y.; Bismarck, A.; Williams, D. R. Anisotropic Surface Chemistry of Crystalline Pharmaceutical Solids. *AAPS PharmSciTech* **2006**, *7*, E12−E20.

(3) Hammond, R. B.; Pencheva, K.; Roberts, K. J.; Auffret, T. Quantifying Solubility Enhancement Due to Particle Size Reduction and Crystal Habit Modification: Case Study of Acetyl Salicylic Acid. *J. Pharm. Sci.* **2007**, *96*, 1967−1973.

(4) Gressl, C.; Brunsteiner, M.; Davis, A.; Landis, M.; Pencheva, K.; Scrivens, G.; Sluggett, G. W.; Wood, G. P. F.; Gruber-Woelfler, H.; Khinast, J. G.; Paudel, A. Drug-Excipient Interactions in the Solid State: The Role of Different Stress Factors. *Mol. Pharmaceutics* **2017**, *14*, 4560−4571.

(5) Hartman, P.; Perdok, W. G. On the relations between structure and morphology of crystals. I. *Acta Crystallogr.* **1955**, *8*, 49−52.

(6) Myerson, A. S.; Ginde, R. *Crystals, Crystal Growth, and Nucleation*; Butterworth-Heinemann: Boston, 1993.

(7) Winn, D.; Doherty, M. F. A new technique for predicting the shape of solution-grown organic crystals. *AIChE J.* **1998**, *44*, 2501−2514.

(8) Clydesdale, G.; Docherty, R.; Roberts, K. J. HABIT - a program for predicting the morphology of molecular crystals. *Comput. Phys. Commun.* **1991**, *64*, 311−328.

(9) Docherty, R.; Roberts, K. J.; Dowty, E. Morang - A computer program designed to aid in the determinations of crystal morphology. *Comput. Phys. Commun.* **1988**, *51*, 423−430.

(10) Lahav, M.; Leiserowitz, L. The effect of solvent on crystal growth and morphology. *Chem. Eng. Sci.* **2001**, *56*, 2245−2253.

(11) Snyder, R. C.; Doherty, M. F. Faceted Crystal Shape Evolution During Dissolution or Growth. *AIChE J.* **2007**, *53*, 1337−1348.

(12) Lovette, M. A.; Browning, A. R.; Griffin, D. W.; Sizemore, J. P.; Snyder, R. C.; Doherty, M. F. Crystal Shape Engineering. *Ind. Eng. Chem. Res.* **2008**, *47*, 9812−9833.

(13) Zhang, Y.; Doherty, M. F. Simultaneous prediction of crystal shape and size for solution crystallization. *AIChE J.* **2004**, *50*, 2101−2112.

(14) Frank, F. C. On the kinematic theory of crystal growth and dissolution processes. In *Growth and Perfection of Crystals*; WILEY-VCH Verlag GmbH & Co.: New York, 1958; p 411.

(15) Chernov, A. The Kinetics of the Growth Forms of Crystals. *Sov. Phys. Crystallogr.* **1963**, *7*, 728−730.

(16) Burton, W. K.; Cabrera, N.; Frank, F. C. The Growth of Crystals and the Equilibrium Structure of their Surfaces. *Philos. Trans. R. Soc., A* **1951**, *243*, 299−358.

(17) Dandekar, P.; Kuvadia, Z. B.; Doherty, M. F. Engineering Crystal Morphology. *Annu. Rev. Mater. Res.* **2013**, *43*, 359−386.

(18) Davey, R. J. The role of the solvent in crystal growth from solution. *J. Cryst. Growth* **1986**, *76*, 637−644.

(19) Zhang, Y.; Sizemore, J. P.; Doherty, M. F. Shape Evolution of 3-Dimensional Faceted Crystals. *AIChE J.* **2006**, *52*, 1906−1915.

(20) Winn, D.; Doherty, M. F. Modeling crystal shapes of organic materials grown from solution. *AIChE J.* **2000**, *46*, 1348−1367.

(21) Lovette, M. A.; Muratore, M.; Doherty, M. F. Crystal Shape Modification Through Cycles of Dissolution and Growth: Attainable Regions and Experimental Validation. *AIChE J.* **2012**, *58*, 1465−1474.

(22) Snyder, R. C.; Studener, S.; Doherty, M. F. Manipulation of Crystal Shape by Cycles of Growth and Dissolution. *AIChE J.* **2007**, *53*, 1510−1517.

(23) Aubrey-Medendorp, C.; Parkin, S.; Li, T. The Confusion of Indexing Aspirin Crystals. *J. Pharm. Sci.* **2008**, *97*, 1361−1367.

(24) Watanabe, A.; Yamaoka, Y.; Takada, K. Crystal Habits and Dissolution Behavior of Aspirin. *Chem. Pharm. Bull.* **1982**, *30*, 2958−2963.

(25) Glasby, J.; Ridgway, K. The crystallization of aspirin from ethanol. *J. Pharm. Pharmacol.* **1968**, *20*, 94S−103S.

(26) Danesh, A.; Davies, M. C.; Hinder, S. J.; Roberts, C. J.; Tendler, S. J. B.; Williams, P. M.; Wilkins, M. J. Surface Characterization of Aspirin Crystal Planes by Dynamic Chemical Force Microscopy. *Anal. Chem.* **2000**, *72*, 3419−3422.

(27) Heng, J. Y. Y.; Bismarck, A.; Lee, A. F.; Wilson, K.; Williams, D. R. Anisotropic Surface Chemistry of Aspirin Crystals. *J. Pharm. Sci.* **2007**, *96*, 2134−2144.

(28) Li, T.; Li, B.; Tomassone, M. S. Surface characterization of aspirin crystal planes using molecular dynamics simulations. *Chem. Eng. Sci.* **2006**, *61*, 5159−5169.

(29) Eder, R. J. P.; Schrank, S.; Besenhard, M. O.; Roblegg, E.; Gruber-Woelfler, H.; Khinast, J. G. Continuous Sonocrystallization of Acetylsalicylic Acid (ASA): Control of Crystal Size. *Cryst. Growth Des.* **2012**, *12*, 4733−4738.

(30) Eder, R. J. P.; Radl, S.; Schmitt, E.; Innerhofer, S.; Maier, M.; Gruber-Woelfler, H.; Khinast, J. G. Crystallization of APIs in a Continuously Seeded Tubular Crystallizer. *Sci. Pharm.* **2010**, *78*, 664.

(31) Eder, R. J. P.; Radl, S.; Schmitt, E.; Innerhofer, S.; Maier, M.; Gruber-Woelfler, H.; Khinast, J. G. Continuously Seeded, Continuously Operated Tubular Crystallizer for the Production of Active Pharmaceutical Ingredients. *Cryst. Growth Des.* **2010**, *10*, 2247−2257.

(32) Besenhard, M. O.; Chaudhury, A.; Vetter, T.; Ramachandran, R.; Khinast, J. G. Evaluation of Parameter Estimation Methods for Crystallization Processes Modeled via Population Balance Equations. *Chem. Eng. Res. Des.* **2015**, *94*, 275−289.

(33) Neugebauer, P.; Khinast, J. G. Continuous Crystallization of Proteins in a Tubular Plug-Flow Crystallizer. *Cryst. Growth Des.* **2015**, *15*, 1089−1095.

(34) Eder, R. J. P.; Schmitt, E.; Radl, S.; Gruber-Woelfler, H.; Khinast, J. G.; Grill, J. Kontinuierliches Wachstum von API Impf- zu Produktkristallen in einem Rohrkristallisator. *Chem. Ing. Tech.* **2010**, *82*, 1469−1470.

(35) Besenhard, M. O.; Thurnberger, A.; Hohl, R.; Faulhammer, E.; Rattenberger, J.; Khinast, J. G. Continuous API-crystal coating via coacervation in a tubular reactor. *Int. J. Pharm.* **2014**, *475*, 198−207.

(36) Besenhard, M. O.; Hohl, R.; Hodzic, A.; Eder, R. J. P.; Khinast, J. G. Modeling a seeded continuous crystallizer for the production of active pharmaceutical ingredients. *Cryst. Res. Technol.* **2014**, *49*, 92−108.

(37) Eder, R. J. P.; Schmitt, E.; Grill, J.; Radl, S.; Gruber-Woelfler, H.; Khinast, J. G. Seed loading effects on the mean crystal size of acetylsalicylic acid in a continuous-flow crystallization device. *Cryst. Res. Technol.* **2011**, *46*, 227−237.

(38) Eder, R. J. P.; Gruber-Woelfler, H.; Khinast, J. G. Kontinuierliche Kristallisation in einem Rohrkristallisator. *Chem. Ing. Tech.* **2009**, *81*, 1171−1171.

(39) Besenhard, M. O.; Neugebauer, P.; Ho, C.-D.; Khinast, J. G. Crystal Size Control in a Continuous Tubular Crystallizer. *Cryst. Growth Des.* **2015**, *15*, 1683−1691.

(40) Besenhard, M. O.; Neugebauer, P.; Scheibelhofer, O.; Khinast, J. G. Crystal Engineering in Continuous Plug-Flow Crystallizers. *Cryst. Growth Des.* **2017**, *17*, 6432−6444.

(41) Maia, G.; Giulietti, M. Solubility of Acetylsalicylic Acid in Ethanol, Acetone, Propylene Glycol, and 2-Propanol. *J. Chem. Eng. Data* **2008**, *53*, 256−258.

(42) Agimelen, O. S.; Jawor-Baczynska, A.; McGinty, J.; Dziewierz, J.; Tachtatzis, C.; Cleary, A.; Haley, I.; Michie, C.; Andonovic, I.; Sefcik, J.; Mulholland, A. J. Integration of in situ imaging and chord length distribution measurements for estimation of particle size and shape. *Chem. Eng. Sci.* **2016**, *144*, 87−100.

(43) *MATLAB and Computer Vision System ToolboxTM*, Release 2016a; The MathWorks, Inc.: Natick, MA, 2016.

(44) *MATLAB and Image Processing Toolbox*, Release 2016a; The MathWorks, Inc.: Natick, MA, 2016.

(45) Schorsch, S.; Vetter, T.; Mazzotti, M. Measuring multidimensional particle size distributions during crystallization. *Chem. Eng. Sci.* **2012**, *77*, 130−142.

(46) Terdenge, L. M.; Heisel, S.; Schembecker, G.; Wohlgemuth, K. Agglomeration degree distribution as quality criterion to evaluate crystalline products. *Chem. Eng. Sci.* **2015**, *133*, 157−169.

(47) de Albuquerque, I.; Mazzotti, M.; Ochsenbein, D. R.; Morari, M. Effect of Needle-Like Crystal Shape on Measured Particle Size Distributions. *AIChE J.* **2016**, *62*, 2974−2985.

(48) Borchert, C.; Sundmacher, K. Crystal aggregation in a flow tube: Image-based observation. *Chem. Eng. Technol.* **2011**, *34*, 545−556.

(49) Borchert, C.; Temmel, E.; Eisenschmidt, H.; Lorenz, H.; Seidel-Morgenstern, A.; Sundmacher, K. Image-Based in Situ Identification of Face Specific Crystal Growth Rates from Crystal Populations. *Cryst. Growth Des.* **2014**, *14*, 952−971.

(50) Faria, N.; Pons, M. N.; Feyo de Azevedo, S.; Rocha, F. A.; Vivier, H. Quantification of the morphology of sucrose crystals by image analysis. *Powder Technol.* **2003**, *133*, 54−67.

(51) Ferreira, A.; Faria, N.; Rocha, F.; Teixeira, J. A. Using an online image analysis technique to characterize sucrose clystal morphology durring a crystallization run. *Ind. Eng. Chem. Res.* **2011**, *50*, 6990−7002.

(52) Flood, A. E. Feedback between crystal growth rates and surface roughness. *CrystEngComm* **2010**, *12*, 313−323.

(53) Pantaraks, P.; Flood, A. E. Effect of Growth Rate History on Current Crystal Growth: A Second Look at Surface Effects on Crystal Growth Rates. *Cryst. Growth Des.* **2005**, *5*, 365−371.